
SPECTROSCOPY ON NANOPARTICLES WITHOUT LIGHT

A PREPRINT

J. Fiedler *

Physikalisches Institut
Albert-Ludwigs-Universität Freiburg
Hermann-Herder-Str. 3
79104 Freiburg, Germany
johannes.fiedler@physik.uni-freiburg.de

C. Persson

Centre for Materials Science and Nanotechnology
Department of Physics
University of Oslo
P. O. Box 1048 Blindern
NO-0316 Oslo, Norway

S. Y. Buhmann †

Physikalisches Institut
Albert-Ludwigs-Universität Freiburg
Hermann-Herder-Str. 3
79104 Freiburg, Germany

October 2, 2019

ABSTRACT

One of the most important tools in modern science is the analysis of electromagnetic properties via spectroscopy. The various types of spectroscopy can be classified by the underlying type of interactions between energy and material. In this paper we demonstrate a new class of spectroscopy based on Casimir interactions between a solid investigated object and a reference surface embedded in an environmental liquid medium. Our main example is based on the measurement of Hamaker constants upon changing the concentration of an intervening two-component liquid, where we demonstrate a possible reconstruction algorithm to estimate the frequency-dependent dielectric function of the investigated particle.

1 Introduction

Spectroscopy in general is a method to investigate a material's properties, in particular its electromagnetic properties for the characterisation of an unknown material with respect to its constituents [1] (type and stoichiometry) and its optical behaviour [2] (such as band gaps in semiconductors). A huge challenge is the experimental determination of the dielectric function $\varepsilon(\omega)$ of a material which is due, on the one hand, to the large range of the electromagnetic spectrum and, on the other hand, to the function being complex-valued. In principle, the measurement of the dielectric function ensues by the excitation of the system at the investigated frequency and measurement of its response. The complexity of such experiments is due to the fact that each spectral range requires a different source for the exciting beam. For instance, measurements in the low frequency range (radio waves), where the electromagnetic wave couples to the states of the core spin, require nuclear magnetic resonance spectroscopy [3, 4, 5], which is followed by micro waves, coupling to the electronic spin states and rotational states, which are investigated via electron paramagnetic resonance spectroscopy [6]. The next spectral range is investigated by Terahertz spectroscopy [7, 8]. Before reaching the visible range, the infrared spectrum has to be investigated via infrared [9] and Raman spectroscopy [10], for instance. In the visible and ultraviolet ranges, ultraviolet-visible spectroscopy [11] or reflection spectroscopy [12] is typically used. Finally, X-ray spectroscopy and gamma spectroscopy [13] complete the spectrum. To conclude, a huge number of different experiments has to be performed to measure the complete dielectric function of a material. The dielectric

*Centre for Materials Science and Nanotechnology, Department of Physics, University of Oslo, P. O. Box 1048 Blindern, NO-0316 Oslo, Norway

†Freiburg Institute for Advanced Studies, Albert-Ludwigs-Universität Freiburg, Albertstr. 19, 79104 Freiburg, Germany

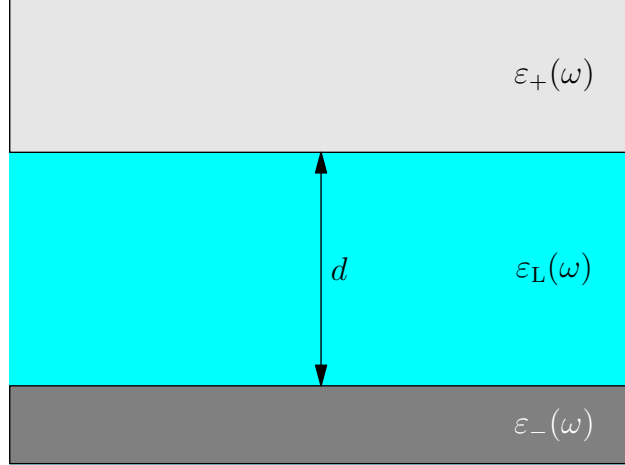


Figure 1: Sketch of Casimir force experiments via atomic force microscopy. A sphere with dielectric function ε_+ and a large curvature radius is attached to a cantilever, which is closely separated from a substrate ε_- . By varying the distance between both objects the Casimir force interacting between them can be measured. In addition to the vacuum experiments a liquid ε_L surrounds the particle.

function being complex poses an additional challenge. For instance, via reflection spectroscopy one usually obtains the real part of the refractive index n and/or the attenuation coefficient k , which is connected with the absorption coefficient. The combination of both results is required to infer the dielectric function. However, often both ingredients are often not simultaneously available and one needs to apply the Kramers–Kronig relation [14, 15], which requires the knowledge of the complete spectrum for the imaginary or real part to calculate the respective other.

However, as we wish to elaborate here, alternatives exist in the form of experiments with a good accuracy whose results directly depend on dynamical dielectric functions, for instance, Casimir experiments via atomic force microscopy in vacuum [16, 17] and in medium [18]. Figure 1 illustrates the typical experimental setup. A spherical nanoparticle is attached to the cantilever of the atomic force microscope. The radius of the sphere should be large enough to neglect effects caused by the curvature of the surface. By changing the distance d between the sphere and the substrate the Casimir force can be measured. In such experiments, one typically uses a sphere of large curvature radius to overcome the issue of arranging two parallel plates and applies the Lifshitz formula for the theoretical description.

In this manuscript, we consider the above mentioned Casimir experiment and show a possible way to extract the dielectric function of one plate from the measured Casimir force data. In order to vary the Casimir force, we assume a liquid surrounding the sphere which consists of two components. Hence, the observed force depends on the concentration of the two liquids. We consider a simple example to illustrate the method with a textbook inversion procedure to infer the dielectric constant from the force data. The method can easily be extended beyond this proof of principle demonstration to improve the precision or generalise to other measurement setups.

2 Theory and reconstruction method

2.1 Casimir effect in media

The Casimir effect, the typically attractive force between two dielectric plates with permittivities ε_- (bottom plate) and ε_+ (top plate) separated by a distance d with a medium permittivity ε_L , can be described via the sum over the exchange of virtual photons between them [19, 20, 21]

$$f(d) = -\frac{k_B T}{\pi} \sum_{m=0}^{\infty} \prime \int_0^{\infty} dk_{\parallel} k_{\parallel} \kappa^{\perp} \sum_{\sigma=s,p} \frac{r_{\sigma}^+ r_{\sigma}^- e^{-2\kappa^{\perp} d}}{D_{\sigma}}, \quad (1)$$

with the Boltzmann constant k_B , the temperature T , the primed sum denotes that the first term has to be weighted by $1/2$, the Matsubara frequencies $\xi_m = m 2\pi k_B T / \hbar$, the multiple reflection terms $D_{\sigma} = 1 - r_{\sigma}^+ r_{\sigma}^- e^{-2\kappa^{\perp} d}$ and the imaginary part of the transverse wave vector $\kappa_i^{\perp} = \sqrt{k_{\parallel}^2 + \varepsilon_i \xi^2 / c^2}$. The coefficients r_{σ}^{\pm} are the generalised reflection

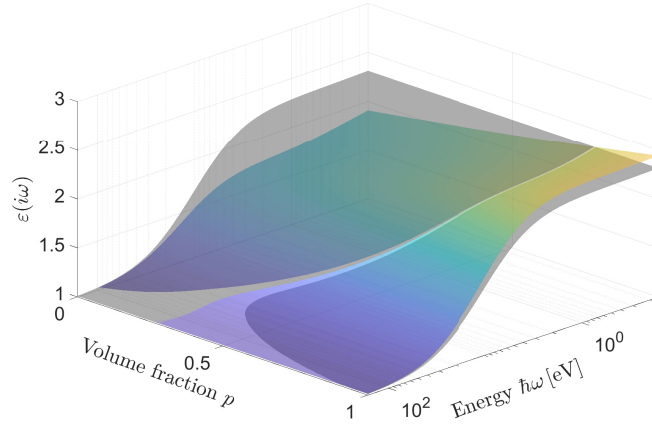


Figure 2: (Color online) Effective dielectric function $\varepsilon_L(i\xi, p)$ of the mixed components methanol and bromobenzene depending on the volume fraction p . In order to illustrate the crossings in the dielectric function the grey surface denotes the permittivity of polystyrene $\varepsilon_-(i\xi)$.

coefficients at the interfaces for p - and s -polarised waves [22, 23]

$$r_p^{i,j} = \frac{\varepsilon_j \kappa_i^\perp - \varepsilon_i \kappa_j^\perp}{\varepsilon_j \kappa_i^\perp + \varepsilon_i \kappa_j^\perp}, \quad r_s^{i,j} = \frac{\kappa_i^\perp - \kappa_j^\perp}{\kappa_i^\perp + \kappa_j^\perp}, \quad (2)$$

respectively. In the non-retarded limit, the z -component of the Casimir force density reads

$$f(d) = -\frac{H}{6\pi d^3}, \quad (3)$$

with the Hamaker constant

$$H = \frac{3k_B T}{2} \sum_{m=0}^{\infty} \frac{\text{Li}_3[r_p^+(i\xi_m) r_p^-(i\xi_m)]}{\varepsilon_L(i\xi_m)}, \quad (4)$$

the polylogarithmic function

$$\text{Li}_3(y) = 4 \int_0^{\infty} dx x^2 \frac{y e^{-2x}}{1 - y e^{-2x}}, \quad (5)$$

and the non-retarded reflection coefficients for p -polarised waves

$$r_p^\pm = \frac{\varepsilon_\pm - \varepsilon_L}{\varepsilon_\pm + \varepsilon_L}. \quad (6)$$

The estimation of the Hamaker constant via this type of experiments is very accurate, which decrease the errors of the reconstruction method as one can assume that the measured Hamaker constants are precisely measured. Current experiments reports on deviations below 5% depending on the reduction of surface roughness, spatial resolution and error of the spring constant [24].

2.2 Mixing of fluids

In order to introduce tunable parameter, we consider a two-component fluid between both plates. For the dielectric functions of mixtures between fluid 1 (ε_1) in fluid 2 (ε_2) we use a Lorentz–Lorenz like model [25]

$$\varepsilon_L = \frac{1 + 2\tilde{\alpha}}{1 - \tilde{\alpha}}, \quad \tilde{\alpha} = p \frac{\varepsilon_1 - 1}{\varepsilon_1 + 2} + (1 - p) \frac{\varepsilon_2 - 1}{\varepsilon_2 + 2}, \quad (7)$$

where p is the volume fraction of fluid 1 in fluid 2. In order to illustrate the results, we choose the liquids bromobenzene and methanol in front of a polystyrene surface [18]. Figure 2 illustrates the resulting dielectric function. One observes a change of the crossings of the dielectric functions depending on the volume fraction by following the intersection of the coloured surface (liquid) and the grey slightly transparent surface (polystyrene).

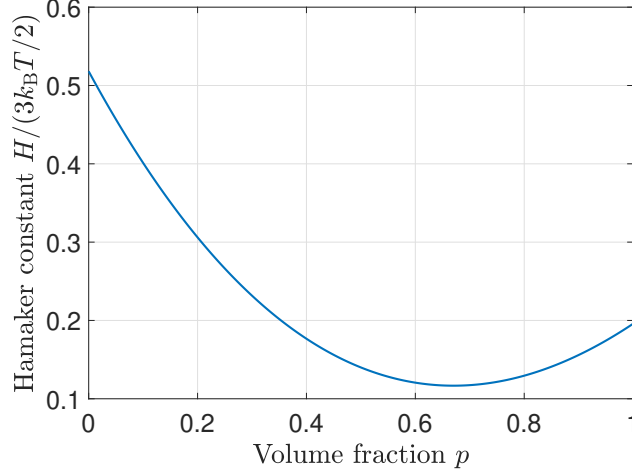


Figure 3: Example of Hamaker constants between two dielectric plates embedded in a two component liquid with the volume fraction p giving the ration of bromobenzene in methanol.

2.3 Repeated measurements with changed concentration

The result of repeated measurements with different concentrations is a series of Hamaker constants

$$H(p) = \frac{3k_B T}{2} \times \sum_{m=0}^{\infty} r^m \frac{1}{\varepsilon_L(p)} \text{Li}_3 \left[\frac{\varepsilon_+ - \varepsilon_L(p)}{\varepsilon_+ + \varepsilon_L(p)} \frac{\varepsilon_- - \varepsilon_L(p)}{\varepsilon_- + \varepsilon_L(p)} \right], \quad (8)$$

with ε_+ being the target dielectric function. In general, this function maps uniquely the target dielectric function onto the set of Hamaker constants, because reflection coefficients are typically bounded by $|r| \leq 1$ which allows for the Taylor series expansion of the polylogarithmic function.

In order to illustrate the reconstruction method, we calculate the Hamaker constants for different volume fraction with a plate, where the target dielectric function to be reconstructed is given by a two-oscillator model

$$\varepsilon_+(i\omega) = 1 + \sum_i \frac{c_i}{1 + (\omega/\omega_i)^2}, \quad (9)$$

with $c_1 = 2$, $c_2 = 1.5$, $\omega_1 = 2$ eV and $\omega_2 = 6$ eV, which are typically values for a dielectric body.

2.4 Reconstruction method

The inverse problem is now defined as calculating the dielectric function of the plate $\varepsilon_+(\omega)$ given the knowledge about the Hamaker constants $H(p)$, the substrate dielectric function $\varepsilon_-(\omega)$ and the liquid dielectric function $\varepsilon_L(p, \omega)$ via Eq. (8). The dielectric function is a linear response function and has to satisfy specific properties, which will be exploited via the reconstruction method. First of all, the dielectric function is to satisfy causality, which leads to the connection of its real and imaginary parts via the Kramers–Kronig relation

$$\text{Re } \varepsilon(\omega) = 1 + \frac{2}{\pi} \mathcal{P} \int_0^{\infty} \frac{\omega' \text{Im } \varepsilon(\omega')}{\omega'^2 - \omega^2} d\omega', \quad (10)$$

$$\text{Im } \varepsilon(\omega) = -\frac{2}{\pi} \mathcal{P} \int_0^{\infty} \frac{\omega' \text{Re } \varepsilon(\omega')}{\omega'^2 - \omega^2} d\omega', \quad (11)$$

with the Cauchy principal value. By substituting $\omega = i\xi$ into (10) the relation to imaginary arguments can be found

$$\varepsilon(i\xi) = 1 + \frac{2}{\pi} \int_0^{\infty} \frac{\omega' \text{Im } \varepsilon(\omega')}{\omega'^2 + \xi^2} d\omega'. \quad (12)$$

Further, the function has to go to 1 for large frequency arguments, $\lim_{\omega \rightarrow \infty} \varepsilon(\omega) = 1$. Another important property is the analyticity in the upper complex half-plane. This fact together with the causality leads to the monotonic behaviour on the imaginary frequency axis. Due to the fact that the dielectric function is a linear response function sum rules exist that also have to be satisfied [26] which are less important for our considerations as we neglect the damping of the response.

The Hamaker constant $H(p)$, which is depicted in Fig. 3 for the material combination with a polystyrene substrate and a bromobenzene and methanol liquid (both depicted in Fig. 2) and the sphere with dielectric function (9), depends non-linearly on the target function ε_+ . Thus, we apply Newton–Raphson method to Eq. (8), that transforms the non-linearity into an iterative algorithm of systems of equations, which needs to be solved in the following way:

(i) initialization, where we choose

$$x_{0,i} = \varepsilon_+^{(0)}(i\omega_i) = 1 + \frac{A}{1 + (\omega_i/B)^2}, \quad (13)$$

along a frequency grid of the first 200 Matzubara frequencies, with the parameters $A = 8$ and $B = 0.5$ eV.

This initial function was chosen in order to ensure the monotonic decreasing of the dielectric function. The stability of the method strongly depends on the value B . For large values, the function overestimates the high-frequency regime too much leading to the convergence to a false (local) minimum. For small values, this region is strongly depressed, stabilising the method. In contrast, the chosen amplitude does not effect the stability of the method. Further, the static dielectric constant is overestimated by $\varepsilon_+^{(0)}(0) = 9$. The target function to be determined only has $\varepsilon_+(0) = 4.5$. Simulations showed that an overestimation of the static value is easier to handle for the algorithm. In order to run the method on an ordinary computer, we restrict ourselves to considering only the first 200 Matsubara frequencies (at room temperature), which covers the spectral range reaching extreme ultraviolet that covers most of the physical effects. This algorithm is followed by

(ii) the calculation of the matrix $D_{ij} = \frac{\partial H(p_i)}{\partial \varepsilon_+(i\omega_j)}$ to solve the system of equations

$$\mathbf{D}\Delta\mathbf{x}^{(i+1)} = H(p) - H(p, \Delta\mathbf{x}^{(i)}), \quad (14)$$

with the measured Hamaker constants $H(p)$ and the calculated Hamaker constants based on the previously iterated data according to Eq. (8).

The matrix \mathbf{D} typically has singularities. To overcome this issue, we applied the Moore–Penrose Pseudoinverse. It is known that Newton’s method converges locally, which means that it strongly depends on the initial data. This effect is directly observable by oscillations in the target function that violates the causality properties of the dielectric function mentioned above. In order to solve this issue, we regularly force the newly iterated function onto a causal monotonic profile by

(iii) fitting the result to a strictly monotonically decreasing function

$$x_j^{(i+1)} = x_j^{(i)} + \Delta x_j^{(i)} \approx 1 + \frac{\lambda_1}{1 + (\omega_j/\lambda_2)^2}, \quad (15)$$

with the parameters $\lambda_{1,2}$.

We find that a fitting to this single oscillator model, which satisfies the monotonic behaviour, works optimal and reproduces the more complicated two-oscillator target after the next iteration. This favourable behaviour is caused by the large differences between the oscillator strengths in the example (9). On smaller scales with two or more narrow peaks, we introduce a termination condition for the filter (iii) according to the iterated step by

(iv) Calculate the maximum iterative step size

$$\max_j |\Delta\varepsilon_+(i\omega_j)| < C, \quad (16)$$

which we chose in our case to be 0.1. By step sizes below this threshold, the fitting step (iii) will be left out.

We also tested the reconstruction method for models with more oscillators and the data were reproduced with less than 100 iterations. The result of this reconstruction method with the target function (9) is depicted in Fig. 4. It can be observed that the target function is reproduced 6 iterations. Especially, the regions around the two oscillators (at 2 eV and 6 eV) are well reproduced. A small deviation of the static value is observed. The presented inversion method has

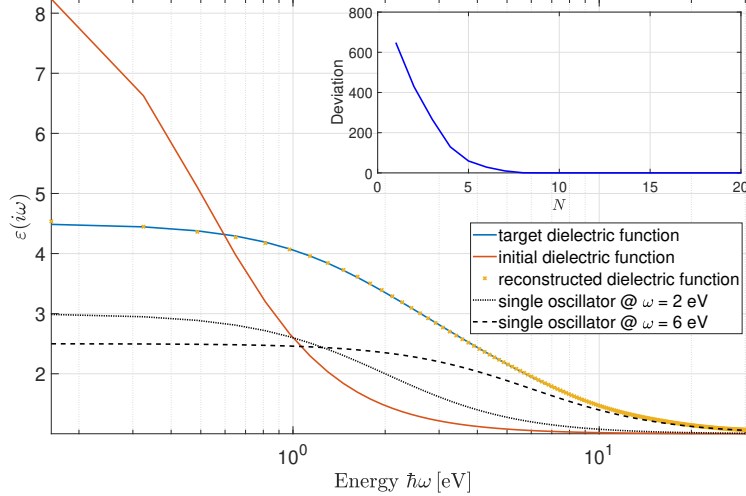


Figure 4: Agreement of the reconstruction method; the target dielectric function (blue solid line) is well-reproduced by the reconstructed dielectric function (yellow crosses). The initial dielectric function (red solid line) illustrates the convergences of the method. In the inlay plot the convergence of the method is depicted via the least square of the target function and the reconstructed function in each iteration step.

some limitations according to the possible reconstruction of completely unknown dielectric functions. In the presented way the target dielectric function has to be quite smooth in order to be approximated by a single oscillator response function with respect to the condition (16). In order to take errors due to this condition into account one needs the redo the calculation with different values. Due to a generalisation of this method to arbitrary response functions, one needs to record the oscillating profiles in between where one observes fix points that already match the target function. Thus, an improvement of the method can be performed with respect to two possibilities: (a) by optimising the fitting in step (iii); or (b) by reducing the system of equations, step (ii), to reproduce these values directly.

After the reconstruction of the target dielectric function on the imaginary frequency axis $\varepsilon_+(i\xi)$, the result needs to be transformed to the real frequency axis. This can be done via the integral equation (10) which is an inhomogeneous Fredholm equation of the first kind. This procedure results in the imaginary part of the dielectric function and after the additional application of the Kramers–Kronig relation (10) its real part can be obtained.

3 Conclusions

We have introduced a reconstruction method to estimate the dielectric function of a solid plate via the established Casimir experiments. In order to estimate the dielectric function along 200 Matsubara frequencies, 200 Hamaker constants at different concentrations are required. For larger distances, the frequency and spatial dependences of the interaction do not separate [27] which can be exploited to reduce the number of experimental repetitions. A more efficient reduction of experiments towards an application of this method can be found via the training of a neuronal network, which will be object of investigation in further studies. Beside the introduced application of the reconstruction of the dielectric function of the attached nanoparticle, the method can directly be used to measure the substrate and after some modification to measure the dielectric function of the liquid. The decomposition of the liquid or gas components will also be part of future investigations. Further, this method can be adapted to low spectral ranges, terahertz radiation and below, where current methods fail, by combining the proposed method with experimentally obtained data from higher energy ranges. By cooling the system down to several Kelvin, the natural discretisation yields roughly 100 points covering the terahertz regime. Further cooling will lead to the transition to the zero-Kelvin Casimir force, where the discrete sum has to be exchanged by the continuous integral which results in a free parameterisation for the investigated regime depending on the knowledge of further optical data. Experimentally challenging is the control of two liquids at the required low temperatures, which can be done by using superfluids or ultracold quantum gases.

Acknowledgments

We acknowledge support from the Research Council of Norway (Project 250346). We gratefully acknowledge support by the German Research Council (grant BU 1803/6-1, S.Y.B. and J.F., BU 1803/3-1, S.Y.B.), the Freiburg Institute for Advanced Studies (S.Y.B.).

References

- [1] Bernhard Welz and Michael Sperling. *Atomic Absorption Spectrometry*. WILEY-VCH, Weinheim, 1998.
- [2] Cecilie S Granerød, Bjørn L Aarseth, Phuong Dan Nguyen, Calliope Bazioti, Alexander Azarov, Bengt G Svensson, Lasse Vines, and Øystein Prytz. Structural and optical properties of individual zn₂geo₄ particles embedded in ZnO. *Nanotechnology*, 30(22):225702, mar 2019.
- [3] F. Bloch and A. Siegert. Magnetic resonance for nonrotating fields. *Phys. Rev.*, 57:522–527, Mar 1940.
- [4] Luis W. Alvarez and F. Bloch. A quantitative determination of the neutron moment in absolute nuclear magnetons. *Phys. Rev.*, 57:111–122, Jan 1940.
- [5] E. M. Purcell, H. C. Torrey, and R. V. Pound. Resonance absorption by nuclear magnetic moments in a solid. *Phys. Rev.*, 69:37–38, Jan 1946.
- [6] E Zavoisky. Paramagnetic absorption in some salts in perpendicular magnetic fields. *Zhurnal Eksperimentalnoi I Teoreticheskoi Fiziki*, 16(7):603–606, 1946.
- [7] F. Junginger, A. Sell, O. Schubert, B. Mayer, D. Brida, M. Marangoni, G. Cerullo, A. Leitenstorfer, and R. Huber. Single-cycle multiterahertz transients with peak fields above 10 mv/cm. *Opt. Lett.*, 35(15):2645–2647, Aug 2010.
- [8] R. Buchner, J. Barthel, and J. Stauber. The dielectric relaxation of water between 0°c and 35°c. *Chemical Physics Letters*, 306(1):57 – 63, 1999.
- [9] C. Christiansen. Untersuchungen über die optischen eigenschaften von fein vertheilten körpern. *Annalen der Physik*, 260(3):439–446, 1885.
- [10] Ingrid De Wolf. Micro-raman spectroscopy to study local mechanical stress in silicon integrated circuits. *Semiconductor Science and Technology*, 11(2):139–154, feb 1996.
- [11] Henrik Stranneheim and Joakim Lundeberg. Stepping stones in dna sequencing. *Biotechnology Journal*, 7(9):1063–1073, 2012.
- [12] Jack L. Koenig. Chapter 3 - experimental ir spectroscopy of polymers. In Jack L. Koenig, editor, *Spectroscopy of Polymers (Second Edition)*, pages 77 – 145. Elsevier Science, New York, second edition, 1999.
- [13] Gordon R. Gilmore. *Practical Gamma-Ray Spectrometry*. John Wiley & Sons, Chichester, 2008.
- [14] R. de L. Kronig. On the theory of dispersion of x-rays. *J. Opt. Soc. Am.*, 12(6):547–557, Jun 1926.
- [15] H.A. Kramers. La diffusion de la lumière par les atomes. *Atti Cong. Intern. Fisici, (Transactions of Volta Centenary Congress)*, 2:545–557, 1927.
- [16] P. S. Davids, F. Intravaia, F. S. S. Rosa, and D. A. R. Dalvit. Modal approach to casimir forces in periodic structures. *Phys. Rev. A*, 82:062111, Dec 2010.
- [17] Peter Loskill, Christian Zeitz, Samuel Grandthyll, Nicolas Thewes, Frank Müller, Markus Bischoff, Mathias Herrmann, and Karin Jacobs. Reduced adhesion of oral bacteria on hydroxyapatite by fluoride treatment. *Langmuir*, 29(18):5528–5533, 2013. PMID: 23556545.
- [18] P. J. van Zwol and G. Palasantzas. Repulsive casimir forces between solid materials with high-refractive-index intervening liquids. *Phys. Rev. A*, 81:062502, Jun 2010.
- [19] Iver Brevik and Simen A. Ellingsen. Comment on “Casimir force acting on magnetodielectric bodies embedded in media”. *Phys. Rev. A*, 79:027801, Feb 2009.
- [20] S. Y. Buhmann. *Dispersion Forces I: Macroscopic quantum electrodynamics and ground-state Casimir, Casimir-Polder and van der Waals forces*. Springer, Heidelberg, 2012.
- [21] Burger, Friedrich Anton, Fiedler, Johannes, and Buhmann, Stefan Yoshi. Zero-point electromagnetic stress tensor for studying Casimir forces on colloidal particles in media. *EPL*, 121(2):24004, 2018.
- [22] M. S. Tomaš. Green function for multilayers: Light scattering in planar cavities. *Phys. Rev. A*, 51:2545–2559, Mar 1995.

- [23] W.C. Chew. *Waves and Fields in Inhomogeneous Media*. Institute of Electrical & Electronics Engineers (IEEE), 1995.
- [24] M. Sedighi, V. B. Svetovoy, and G. Palasantzas. Casimir force measurements from silicon carbide surfaces. *Phys. Rev. B*, 93:085434, Feb 2016.
- [25] D. E. Aspnes. Local-field effects and effective-medium theory: A microscopic perspective. *American Journal of Physics*, 50(8):704–709, 1982.
- [26] Claudia Ambrosch-Draxl and Jorge O. Sofo. Linear optical properties of solids within the full-potential linearized augmented planewave method. *Computer Physics Communications*, 175(1):1 – 14, 2006.
- [27] Johannes Fiedler, Wijnand Broer, and Stefan Scheel. Reconstruction of casimir—polder interactions from matter-wave interference experiments. *Journal of Physics B: Atomic, Molecular and Optical Physics*, 50(15):155501, jul 2017.